Mirror-aided Approach for Surface Flatness Inspection using Laser Scanning

Fangxin Li[a] and Min-Koo Kim[b*]

[a] Department of Building and Real Estate, Hong Kong Polytechnic University, Hong Kong SAR
[b]Department of Architectural Engineeringe, Chungbuk National University, Korea
E-mail: fangxin.li@connect.polyu.hk, joekim@cbnu.ac.kr

Abstract –

Surface flatness is an essential indicator for quality assessment of concrete surfaces in the construction industry. Terrestrial laser scanning (TLS) has been popularly applied for surface flatness inspection due to its speed and accuracy. However, scanning area far away from the TLS usually suffers from inaccurate surface flatness measurement and physical barriers such as interior walls are likely to cause occlusion for the surface flatness inspection. To address these limitations, this study proposes a mirror-aided technique for surface flatness inspection. There are two concepts proposed from the mirror-aided technique. First, the mirror-aided approach can address the low accuracy of surface flatness inspection caused by long scanning range and high incident angle, which enlarge the scanning area and increase the surface flatness inspection efficiency. Second, the mirror-aided approach can measure the flatness of the concrete surfaces occluded by barriers based on the mirror reflection principle with one single scan, resulting in efficient surface flatness inspection. To validate the proposed two concepts, a series of tests on laboratory-scale specimens are conducted. The results show that the proposed method provide accurate surface flatness estimation results with an accuracy of more than 85% for the scanning area far away from the TLS and concrete surfaces with occlusion problem, demonstrating the great potential for the application of mirror-aided surface flatness inspection in the construction industry.

Keywords –

Surface flatness; quality inspection; terrestrial laser scanner (TLS); mirror-aided laser scanning

1 Introduction

Surface flatness is an essential checklist for dimensional quality inspection of construction elements and construction floors after manufacturing and construction in the construction industry [1,2,3]. This is because concrete surfaces which have unacceptable deviation from specific tolerance can seriously effect both aesthetic and functional performance of target structures [3,4,5]. Furthermore, the serious non-flatness concrete surfaces are likely to influence subsequent construction and cause poor connection between adjacent elements, resulting in deteriorated structural problem in long term [3,6]. Therefore, it is necessary to implement surface flatness inspection after production to evaluate the flatness quality of the target structure. Currently, surface flatness of concrete surfaces is commonly inspected manually using straightedges in the construction industry [10]. As for straightedge approach, inspectors use a long straightedge to assess surface flatness based on certain measurement patterns, such as grid, to define the gap between the surface and straightedge [1,10]. However, the existing flatness assessment methods have limitations in terms of time consumption, labor intensity and low measurement accuracy.

3D laser scanning has been widely used as a promising data acquisition technology for the purpose of surface flatness inspection of concrete surfaces [11-14]. This is because 3D laser scanning could provide accurate and dense 3D scan points efficiently for surface flatness inspection [15,16]. However, scanning area far away from the TLS usually has large scanning distance and high incident angle, which decrease the accuracy of the surface flatness inspection. Furthermore, construction components are likely to cause occlusion of the floor, which limits the scanning area of the floor. To address these limitations, this study aims to 1) propose a mirror-aided technique for surface flatness inspection to address the low accuracy of the scanning area far away from the TLS and occlusion problems caused by barriers 2) validate the applicability of the mirror-aided flatness inspection technique. The organization of the paper is as follow. The two concepts of the proposed mirror-aided techniques are described in Section 2, followed by validation tests and experiment results in Section 3 and Section 4. Finally, this paper

ends with a brief summary and suggestions for further work in Section 5.

2 Overall concept of mirror-aided approach for surface flatness inspection using laser scanning

Figure 1 shows the overall concepts of mirror-aided approach. Figure 1(a) illustrates the concept of the mirror-aided technique to increase the accuracy of the scanning area far away from the TLS. Here, the scanning area far away from the TLS has large scanning distance and high incident angle (θ). Therefore, the accuracy of the surface flatness inspection for the scanning area far away from the TLS is low, which limits the scanning area of the floor. As for the mirror-aided approach, the flat mirror is located at the backward of the target area far away from the TLS with a certain angle to the ground. The laser beam emitted from the TLS is first reflected by the mirror and then reaches on the scanning area, resulting in a lower incident angle (β). In this way, the mirror-aided approach can increase accuracy of surface flatness inspection caused by large scanning distance and high incident angle, which enlarge the scanning area and increase the surface flatness inspection efficiency. Also, there are rectangular patches attached on the surfaces of flat mirrors to obtain scan points falling onto the patches. Based on the mirror reflection principle [11], the scan points of actual surface obtained from the mirror will be located on the virtual surface. Also, note that the virtual surface and actual surface on the floor are symmetric with respect to the mirror. Figure 1(b) illustrates the concept of the mirror-aided technique to address the occlusion problems caused by barriers. The structural components such as the interior wall are likely to cause occlusion of the floor, which limits the scanning area of the TLS. Therefore, it requires multiple scans to perform the data collection, which deteriorates the surface flatness inspection efficiency. To address the limitation, the mirror is applied to adjust the direction of the laser beam, enabling the scanning of the occlusion area of the floor. In this way, the mirror-aided approach can measure the flatness of the floors based on mirror reflection principle with one single scan, resulting in efficient surface flatness inspection.

3 Materials and test setup

In order validate the two concepts of the mirror aided approach for surface flatness inspection, two experiments named as 'Experiment I' and 'Experiment II' of laboratory-tests were conducted on two specimens. The specific objectives of 'Experiment I' and

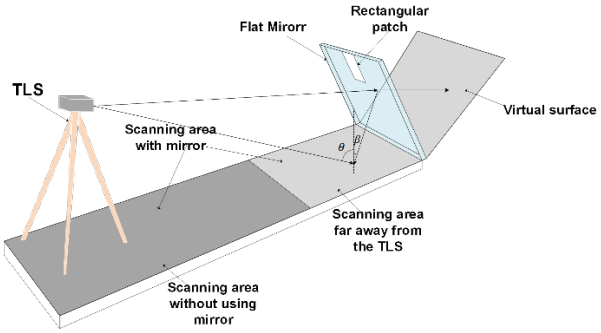

(a)

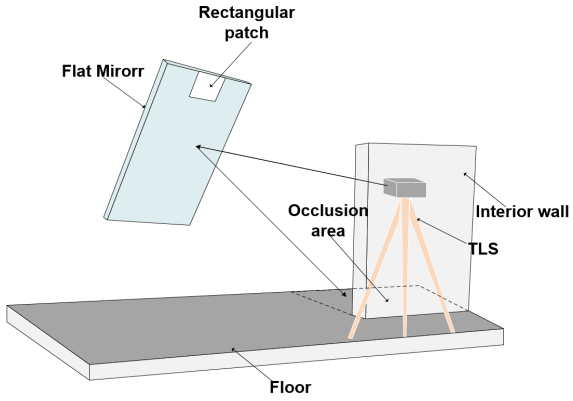

(b)

Figure 1. Overall concepts of mirror-aided approach: (a) the concept of the mirror-aided technique to increase the accuracy of the scanning area far away from the TLS and (b) the concept of the mirror-aided technique to address the occlusion problems

'Experiment II' are : 1) to validate that the mirror-aided approach can increase surface flatness inspection accuracy of the area with large scanning distance and high incident angle, 2) to validate the mirror-aided approach can address the occlusion problem caused by construction components for surface flatness inspection, respectively. Figure 2 shows the two specimens named as 'Specimen I' and 'Specimen II' for the validation experiments. The two specimens were manufactured by a ZRAPID iSLA880 3D printer [17] with the material of photopolymer resin. Table 1 shows the dimensions and F_F numbers of the specimens. Specimen I was manufactured with a size of 400 mm (length) × 400 mm (width)× 10-23 mm (height) and has an F_F number of 10.28. Specimen II, which is flatter than the Specimen I, was sized at 400 mm × 400 mm× 20-38 mm and has an F_F number of 21.23. Note that the size of the mirrors is 1000 mm (length) × 1000 mm (height). In this study, a phase-shift TLS, FARO M70 [18], with an accuracy of ±3 mm at 20 m, was used to acquire scan points of the specimen.

Table 1. Dimensions and F_F numbers of the specimens

Items	Size (length × width × height)	F_F number
Specimen I	400 mm×400 mm×10-23 mm	10.28
Specimen II	400 mm×400 mm×20-38 mm	21.23

(a) (b)

Figure 2. Test specimens for the validation experiments: (a) Specimen I and (b) Specimen II

3.1 Experiment I

3.1.1 Experiment set-up

Figure 3 shows the experimental configuration of Experiment I. The height distance of the TLS was set to 1.5 m and scanning distance was adjusted from 2.5 m to 12.5 m with an interval of 2.5 m. Besides, the mirror was rotated based on the bottom line with an angle of 75° to the ground and there was a gap of 0.35 m between the mirror bottom line and the specimen. On the other hand, two rectangular patches of 100 mm × 100 mm in size were attached to the upper-side region of the mirrors. In addition, three different angular resolutions of 0.036°, 0.072°, and 0.144° were used to investigate the effect of angular resolution. Note that the estimation error of F_F number is defined as the difference between the estimated F_F number of the proposed technique and the designed F_F number of the specimen. Also, note that scan points of the surface which are directly falling on the specimen are called 'actual scan points' and the scan points obtained on the virtual surface through the mirror are called 'virtual scan points' hereafter.

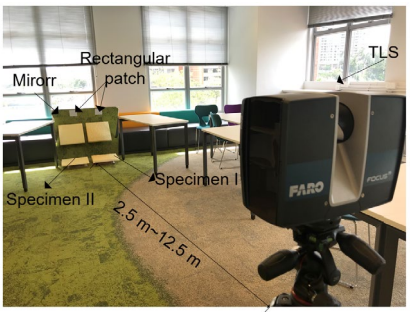

Figure 3. Test configuration of experiment I

3.1.2 Data processing

There are four procedures for the proposed mirror-aided surface flatness inspection technique after data acquisition, which are (1) data pre-processing, (2) virtual scan points transformation, (3) coordinate transformation and (4) surface flatness estimation. First, background noise is removed to extract the scan points corresponding to the specimen and the rectangular patch. Next, using the estimated mirror plane estimated from the scan points of the rectangular patch, the virtual scan points of the specimen surface are transformed to the position of actual scan points. Finally, surface flatness is estimated based on F_F number method [10]. Figure 4 shows the determination of F_F number of a test surface. The detailed procedure of determining the F_F number of a test surface according to ASTM E 1155 (ASTM 2008) [10] is illustrated as the following 5 steps.

Step 1: Determination of the sample measurement lines on the test surface. The orientations of the lines should all be parallel, perpendicular or 45° to the longest boundary. In addition, equal number of lines should be placed in two perpendicular directions. Furthermore, the lengths of lines should not be smaller than 3,300 mm and the distance between two parallel lines should not be smaller than 1,200 mm. Step 2: Subdivision of the sample measurement lines. Each sample measurement is divided into 300 mm long intervals and the points marking the ends of these intervals are named 'sample reading points'. Step 3: Measurement of the elevations of the sample reading points (or the elevation difference between all adjacent sample reading points). For sample measurement line j, denote all sample reading points along it as P_0 and P_1, and P_2 and P_3, ... P_{i-1} and P_i, etc. Then, the evaluations between the corresponding reading points are designated as h_0 and h_1, and h_2 and h_3, ... h_{i-1} and h_i accordingly. Step 4: Calculate the F_F number of each sample measurement line. For sample measurement line j, calculate the profile curvatures, q_i, between all sample reading points separated by 600 mm as $h_i - 2h_{i-1} + h_{i-2}$, where i = 2, 3, 4 … n. Subsequently, the F_F number of sample measurement line j, denoted as F_j, is estimated by Eq. (1).

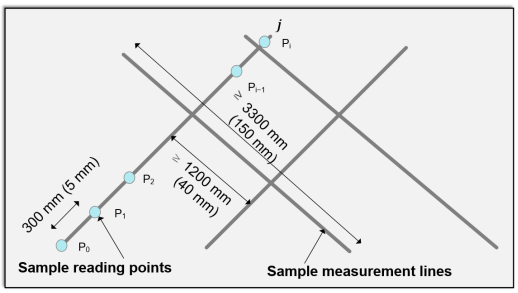

Figure 4. Determination of the F_F number of a test surface

$$F_j = \frac{115.8454}{3S_{qi} + |q_i|} \quad (1)$$

where S_{qi} and $|q_i|$ denote the standard deviation and the absolute value of the mean of all $(n-1)$ q_i values, respectively. Step 5: Calculate the F_F number of the test surface by combining all of the F_F numbers of individual sample measurement lines within the test surface. Considering the limitation of the size of the test specimen, the length of measurement lines and the distance between two parallel measurement lines in this study are selected as 150 mm and 40 mm respectively. In addition, the intervals which separate the sampling reading points is set as 5 mm and the profile curvatures, q_i, is calculated between all sample reading points separated by 10 mm. Since the F_F number is calculated based on the collected scan points, the elevation of each sample reading point will be obtained with the nearest laser scan point. Then, in order to improve the reliability of the results, F_F number is calculated as the average value of the results that is calculated iteratively in 1000 times. For each time, the number of the sample measurement lines and the relative locations between each measurement line are unchanged. As for the distances from the sample measurement lines to the surface boundaries, these values vary in every iteration and is determined by a random number.

3.2 Experiment II

3.2.1 Experiment set-up

In order to validate the concept 2, the height distance of the TLS was set to 2.5 m and scanning distance from the TLS to the mirror and the specimen were 2 m and 1.5 m respectively. Figure 5 shows the test configuration of Experiment II. Besides, barriers were located between the TLS and specimen to make the specimen invisible from the TLS. In addition, a mirror with the size of 1000 mm × 1000 mm was located behind the specimen with a gap of 0.2 m. Here, the center point of the mirror is the pivot point of the rotation and the mirror was aided by a goniometer to achieve rotation in the horizontal and vertical direction. In this experiment, the vertical mirror rotation angle and horizontal mirror radiation angle were set as 20° and 30° respectively. On the other hand, two rectangular patches of 100 mm × 100 mm in size were attached to the upper-side region of the mirrors for mirror plane estimation. In addition, three different angular resolutions of 0.036°, 0.072°, and 0.144° were used to investigate the effect of angular resolution.

Figure 5. Test configuration of Experiment II

3.2.2 Data processing

The data processing process is similar to the experiment I and the only difference is that noise removal. In experiment II, there is no need to extract the virtual scan points of specimen because it cannot be scanned from the TLS.

4 Result and discussion

4.1 Experiment I result and discussion

Table 2 shows the estimation errors of F_F number under varying angular resolutions with different scanning distances. There are three distinctive observations from the results.

First, the estimation errors of F_F number from the scan points are decreased as the scan density increases. Note that the data density is presented as the number of scan points captured each square centimetre. Here, the estimation errors of F_F number under different scan densities from virtual can points are taken as an example to illustrate the effects of scan density on estimation errors. As the scan density increases from 0.3 pts/ cm^2 to 87.7 pts/ cm^2, the estimation error in percentage is decreased from 318.8% to 3.9%. It is also observed that the F_F number cannot be estimated when the scan density is less than 0.2 / cm^2 since the measurement lines are not able to be sampled in sparse scan points for F_F number estimation. In addition, it is also noticed that scan density which excess 5.5 pts /cm^2 are likely to result in accurate F_F number estimation, resulting in error in percentage of less than 20%. However, the actual scan points directly acquired from the TLS usually has low scan density caused by the large scanning distance and high incident angle, which cause low estimation accuracy for surface flatness inspection.

Second, the mirror-aided method can achieve the improvement of 81.5% in accuracy for surface flatness inspection compared to actual scan points under scanning distance of 10 m, addressing the low accuracy of surface flatness inspection caused by large scanning distance and high incident angle. This is because the proposed mirror-aided approach can adjust the incident

Table 2. Estimation errors for F_F number under varying angular resolutions with different scanning distances

Object	Scanning distance (incident angle)	Estimation error of F_F number for Specimen I in percentage (Data density: pts/cm^2)			Estimation error of F_F number for Specimen II in percentage (Data density: pts/cm^2)		
		Angular resolution			Angular resolution		
		0.036°	0.072°	0.144°	0.036°	0.072°	0.144°
Virtual scan points	2.5m (51°)	9.5% (87.7)	13.8% (21.9)	17.1% (5.6)	3.9% (87.2)	8.4% (21.9)	19.9% (5.5)
	5m (43°)	9.6% (27.0)	11.1% (6.7)	91.6% (1.7)	4.0% (27.1)	19.1% (6.7)	29.1% (1.7)
	7.5m (40°)	18.6% (12.7)	37.1% (3.2)	71.2% (0.8)	8.9% (12.9)	11.7% (3.2)	24.1% (0.8)
	10m (38°)	15.1% (7.3)	49.0% (1.8)	183.5% (0.5)	19.8% (7.3)	23.3% (1.8)	48.1% (0.5)
	12.5m (37°)	31.1% (4.9)	49.1% (1.2)	318.8% (0.3)	20.9% (4.8)	37.0% (1.2)	69.6% (0.3)
Actual scan points	2.5m (70°)	19.9% (67.3)	36.1% (16.6)	65.2% (4.5)	4.4% (64.9)	27.0% (16.6)	23.8% (4.2)
	5m (79°)	82.5% (10.6)	83.1% (2.7)	152.9% (0.6)	19.8% (10.6)	19.5% (2.5)	64.1% (0.6)
	7.5m (82°)	161.4% (3.6)	140.5% (0.9)	- (0.2)	58.7% (3.3)	88.4% (0.8)	- (0.2)
	10m (84°)	211.1% (1.5)	278.8% (0.4)	- (<0. 1)	107.3% (1.4)	143.0% (0.3)	- (<0. 1)
	12.5m (86°)	210.3% (0.7)	- (0. 2)	- (<0. 1)	155.6% (0.6)	-(0.2)	- (<0. 1)

angle of laser beam and address the low-density scan points caused by the long scanning range and high incident angle. Due to the long scanning range and high incident angle, the actual scan points which are directly acquired from the specimen are not able to provide accurate results (with error in percentage of less than 20%) when the scanning distance is larger than 5 m. However, the scan density of virtual scan points are around 2 to 4 times that of actual scan points in the same circumstance. Therefore, the mirror-aided approach can acquire accurate result with the scanning distance of 10 m, which enlarge scanning area and increase the efficiency for surface flatness inspection.

Third, Specimen II achieves more accurate F_F number estimation results than Specimen I in most cases, indicating that the mirror-aided approach is more robust for flatness inspection of flatter surfaces. This phenomenon is caused by that the Specimen I with non-flatter surface as shown in Figure 2 is more likely to suffer from the effect of the high incident angle compared to Specimen II with relative flatter surface. Hence, the proposed mirror-aided approach can be effectively applied for floor surface flatness inspection since the concrete floor normally has relative flatter surface.

In summary, the mirror-aided approach can adjust the incident angle of laser beam to address the low measurement caused by the large scanning distance and high incident angle. Therefore, the mirror-aided approach is able to acquire accurate F_F number estimation for surface flatness inspection within a large scanning distance, which enlarge scanning area and increase data collection efficiency.

4.2 Experiment II result and discussion

Table 3 shows the mirror-aided F_F number estimation errors under varying angular resolutions for specimens with occlusion problem. The average errors for Specimen I and Specimen II in percentage are 22.4% and 11.6% respectively, which indicates the applicability of the proposed mirror-aided method for concept 1. This is because that the mirror-aided method adjusts the laser beam direction, enabling the scanning of the specimen occluded by barriers. Moreover, Specimen II achieves more accurate F_F number estimations than Specimen I in most cases since flatter surface of Specimen II is more robust to incident angle

Table 3. Mirror-aided F_F number estimation errors under varying angular resolutions with different scanning distances with occlusion

Object	F_F number estimation error of Specimen I (mm)				F_F number estimation error of Specimen II (mm)			
	Angular resolution				Angular resolution			
	0.036°	0.072°	0.144°	Ave.	0.036°	0.072°	0.144°	Ave.
Discrepancy	1.10	2.84	3.97	2.30	2.21	2.51	2.69	2.47
Discrepancy in percentage	10.7%	27.6%	38.6%	22.4%	10.4%	11.8%	12.6%	11.6%

influence compared to non-flatter surface of Specimen I.

5 Conclusion

This study presents a mirror-aided technique for surface flatness inspection to address low accuracy of the scanning area far from TLS and occlusion problems caused by barriers. First, the mirror-aided approach can increase the low accuracy of surface flatness inspection caused by large scanning distance and high incident angle, which enlarge the scanning area and increase the surface flatness inspection efficiency. The validation results showed that the mirror aided approach can improve the surface flatness inspection accuracy in 81.5%, which address the low accuracy caused by large scanning distance and high incident angle. Second, the mirror-aided approach can measure the flatness of the floors occluded by structural components based on mirror reflection principle with one single scan, resulting in efficient surface flatness inspection. Based on the proposed two concepts, the validation experiments are conducted on two laboratory-scale specimens. From the validation results, the proposed mirror-aided approach achieves an accuracy of more than 85% for Experiment II, indicating the applicability of the proposed mirror-aided approach to address occlusion problems.

However, there are limitations which are left for further study in the near future. First, the test specimens used in this study are lab-scale, so further study is necessary in order to investigate the applicability of the proposed technique to large-scale or full-scale elements. Second, the large-scale mirrors are fragile and take large space which may not be available for extremely large-scale environment.

Acknowledgement

This work is supported by the Korea Agency for Infrastructure Technology Advancement (KAIA) grant funded by the Ministry of Land, Infrastructure and Transport (Grant 20SMIP-A157453-01).

References

[1] British Standards Institution (BSI). BS 8204 — Screeds, Bases and In Situ Flooring (2009)

[2] American Concrete Institute (ACI). ACI 302.1R-96 — Guide for Concrete Floor and Slab Construction (1997)

[3] Park, H. S., Lee, H. M., Hojjat, A., and Lee, I. A new approach for health monitoring of structures: Terrestrial laser scanning. *Computer-aided Civil and Infrastructure Engineering*, 22(1), 19–30, 2007.

[4] Shih, N. J., and Wang, P. H. Using point cloud to inspect the construction quality of wall finish. In *Proceedings of the 22nd eCAADe Conference, pages* 573-578, 2004.

[5] Li, D., Liu, J., Feng, L., Zhou, Y., Liu, P., and Chen, Y. F. Terrestrial Laser Scanning Assisted Flatness Quality Assessment for Two Different Types of Concrete Surfaces. *Measurement*, 107436, 2020.

[6] Wacker, J.M., Eberhard, M.O. and Stanton, J.F. State-of-the-art Report on Precast Concrete Systems for Rapid Construction of Bridges (No. WA-RD 594.1). Washington State Department of Transportation, 2005.

[7] Wang, Q., Kim, M. K., Sohn, H., and Cheng, J. C. Surface flatness and distortion inspection of precast concrete elements using laser scanning technology. *Smart Structures and Systems*, 18(3), 601-623, 2016.

[8] Bosché, F., and Guenet, E. Automating surface flatness control using terrestrial laser scanning and building information models. *Automation in construction*, 44, 212-226, 2014.

[9] Hieber, D. G., Wacker, J. M., Eberhard, M. O., and Stanton, J. F. State-of-the-art report on precast concrete systems for rapid construction of bridges (No. WA-RD 594.1). *Washington State Transportation Center*,2015.

[10] ASTM, ASTM E 1155-96 —Standard Test Method for Determining FF Floor Flatness and FL Floor Levelness Numbers, 2008.

[11] Kim, M. K., Wang, Q., Yoon, S., and Sohn, H., A mirror-aided laser scanning system for geometric quality inspection of side surfaces of precast concrete elements. *Measurement*, 141, 420-428, 2019.

[12] Kim, M. K., Thedja, J. P. P., and Wang, Q., Automated dimensional quality assessment for formwork and rebar of reinforced concrete components using 3D point cloud dat. *Automation in Construction*, 112, 103077, 2020.

[13] Kim, M. K., Wang, Q., and Li, H., Non-contact sensing based geometric quality assessment of buildings and civil structures: A review. *Automation in Construction*, 100, 163-179, 2019.

[14] Wang, Q., and Kim, M. K., Applications of 3D point cloud data in the construction industry: A fifteen-year review from 2004 to 2018. *Advanced Engineering Informatics*, 39, 306-319, 2019.

[15] Wang, Q., Tan, Y., and Mei, Z., Computational methods of acquisition and processing of 3D point cloud data for construction applications. *Archives of Computational Methods in Engineering*, 27(2), 479-499, 2020.

[16] Josephson, P. E., and Hammarlund, Y., The causes and costs of defects in construction: A study of seven building projects. *Automation in Construction*, 8(6): 681-687, 1999.
[17] ZRAPID SLA 3D Printer. Available from: http://www.zero-tek.com/en/sla880.html.
[18] FARO. FARO® LASER SCANNER FOCUS. Available from: https://www.faro.com/en-sg/products/construction-bim/faro-laser-scanner-focus/.